

Silver Nanoparticles as an Effective Antimicrobial against Otitis Media Pathogens

Rong Yang¹, Xiaojing Ma¹, Jiayan Lang¹, and Pengyu Chen¹

¹Cornell University

June 13, 2021

Abstract

Otitis Media (OM) is the most common reason for U.S. children to receive prescribed oral antibiotics, leading to potential to cause antibiotic resistance. To minimize oral antibiotic usage, we developed polyvinylpyrrolidone-coated silver nanoparticles (AgNPs-PVP), which completely eradicated common OM pathogens, i.e., *Streptococcus pneumoniae* and non-typeable *Haemophilus influenzae* (NTHi) at 1.04 μ g/mL and 2.13 μ g/mL. The greater antimicrobial efficacy against *S. pneumoniae* was a result of the H₂O₂-producing ability of *S. pneumoniae* and the known synergistic interactions between H₂O₂ and AgNPs. To enable the sustained local delivery of AgNPs-PVP (e.g., via injection through perforated tympanic membranes), a hydrogel formulation of 18%(w/v)P407 was developed. Reverse thermal gelation of the AgNPs-PVP-P407 hydrogel could gel rapidly upon entering the warm auditory bullae and thereby sustained release of antimicrobials. This hydrogel-based local delivery system completely eradicated OM pathogens in vitro without cytotoxicity, and thus represents a promising strategy for treating bacterial OM without relying on conventional antibiotics.

Silver Nanoparticles as an Effective Antimicrobial against Otitis Media Pathogens

Authors: Xiaojing Ma¹, Jiayan Lang¹, Pengyu Chen¹, Rong Yang^{1*}

Affiliations:

¹ Robert F. Smith School of Chemical & Biomolecular Engineering, Cornell University, Ithaca, NY 14850, USA

* corresponding author. Email: ryang@cornell.edu

Abstract

Otitis Media (OM) is the most common reason for U.S. children to receive prescribed oral antibiotics, leading to potential to cause antibiotic resistance. To minimize oral antibiotic usage, we developed polyvinylpyrrolidone-coated silver nanoparticles (AgNPs-PVP), which completely eradicated common OM pathogens, i.e., *Streptococcus pneumoniae* and non-typeable *Haemophilus influenzae* (NTHi) at 1.04 μ g/mL and 2.13 μ g/mL. The greater antimicrobial efficacy against *S. pneumoniae* was a result of the H₂O₂-producing ability of *S. pneumoniae* and the known synergistic interactions between H₂O₂ and AgNPs. To enable the sustained local delivery of AgNPs-PVP (e.g., via injection through perforated tympanic membranes), a hydrogel formulation of 18%(w/v)P407 was developed. Reverse thermal gelation of the AgNPs-PVP-P407 hydrogel could gel rapidly upon entering the warm auditory bullae and thereby sustained release of antimicrobials. This hydrogel-based local delivery system completely eradicated OM pathogens in vitro without cytotoxicity, and thus represents a promising strategy for treating bacterial OM without relying on conventional antibiotics.

Key Words: silver nanoparticles, infectious disease treatment, otitis media, drug delivery, polyvinylpyrrolidone (PVP)

Introduction

Otitis media (OM), the infection and subsequent inflammation of the middle ear, is the most common illness within the first 24 months of birth¹. By age 5, over 95% of children in the U.S. have had at least one episode of OM^{2,3}. In particular, 58% OM episodes are due to bacterial infections caused by gram-positive *Streptococcus pneumoniae* (*S. pneumoniae*) and/or gram-negative non-typeable *Haemophilus influenzae* (NTHi)^{4,5}, pathogens that commonly colonize the nasopharynx and invade the auditory bullae opportunistically to cause OM⁶.

Oral antibiotic therapy is the current mainstay of treatment for OM. A typical course of treatment comprises 7-10 days of multidose antibiotic regimens⁷. As a result, OM represents the most common reason for pediatric antibiotic prescriptions written to US children^{2,3}. The level of systemic antibiotic exposure caused by OM is further exacerbated by identified antibiotic resistance of OM pathogens. For example, *S. pneumoniae*, responsible for over 30% of all OM cases, is known to have greater tolerance for β -lactam and macrolide^{8,9}. Even with effective fluoroquinolones such as ciprofloxacin, the minimum inhibitory concentration (MIC) of *S. pneumoniae* is as high as 0.5 – 4 $\mu\text{g}/\text{mL}$ ^{10,11}. Effective eradication of *S. pneumoniae* OM requires high antibiotic concentrations in the middle ear, sustained throughout the treatment by adhering to the rigorous multidose oral regimens. The high levels of systemic antibiotic exposure often cause side effects, such as diarrhea, vomiting, and oral thrush¹², which in turn make it challenging to continue the treatment and potentially lead to recurrent OM and wide-spread antibiotic resistance.

In this report, silver nanoparticles (AgNPs) were examined as a potential treatment for the OM pathogens. Contrary to small-molecule antibiotics, we found AgNPs [stabilized with polyvinylpyrrolidone (PVP)] to be highly efficacious against *S. pneumoniae*, with MICs lower than that of NTHi, showing a great potential as a broad-spectrum therapy for OM. In recent years, AgNPs have become an attractive alternative to antibiotics due to their excellent antibacterial effects against both gram-positive and gram-negative pathogens¹³ and even bacteria with multidrug resistance¹⁴. Several mechanisms have been considered to explain the antimicrobial efficacy of AgNPs¹⁵. In brief, AgNPs have been observed to attach to the cell membrane of bacteria, leading to critical damages such as membrane penetration and disabled membrane functions such as respiration (due to deactivation of membrane-bound essential enzymes such as respiratory chain dehydrogenases)^{16,17}, which in turn increases bacterial membrane permeability^{18,19}. AgNPs that penetrated a bacterial cell can damage DNA and deactivate intracellular enzymes^{18,20}, leading to rapid cell death²¹. Furthermore, AgNPs are known to generate reactive oxygen species (ROS) including superoxide anion ($\text{O}_2^{\bullet-}$), hydroxyl radical (OH^{\bullet}), and hydrogen peroxide (H_2O_2)²². The excess ROS produced by AgNPs often deplete glutathione (GSH), an antioxidant produced by virtually all living organisms^{23,24}, and subsequently damage cell membrane and intracellular organisms^{23,24}. Nevertheless, AgNPs have been demonstrated to cause minimal cytotoxicity or immunological responses²⁵ and have thus been adopted across a range of biomedical applications, including drug delivery (e.g., wound healing²⁶, eye infection caused by *Pseudomonas aeruginosa*²⁷, and post-cardiac surgery mediastinitis²⁸) and medical imaging (e.g., human oral cancer²⁹ and multimodality cancer³⁰). Although efficacy of AgNPs against OM pathogens has not been studied previously, we hypothesized that AgNPs could be highly potent, especially against the resistant bacteria *S. pneumoniae*. That hypothesis was based on the potential synergistic interactions between AgNPs and H_2O_2 due to their Fenton-like reactions and the H_2O_2 -generating ability of *S. pneumoniae*³¹⁻³³.

A hydrogel delivery system was designed to enable the localized and sustained presence of AgNPs during the course of the treatment. This design enables an AgNPs-containing formulation to be administered through a perforated tympanic membrane as a liquid, which quickly turns into a firm solid gel to achieve sustained antimicrobial effects. Reverse thermal gelation, the property that enables liquid-phase administration of the formulation at room temperature and rapid gelation at elevated temperature (e.g., body temperature), was achieved using poloxamer 407 (P407)^{34,35}. It enables a single-dose administration into the middle ear with ease and, once in place, prolonged presence of the formulation to prevent recurrent OM. Furthermore,

P407 has been tested as mucoadhesive formulations in rectal delivery of a range of therapeutics such as tizanidine HCl (TIZ) (for treatment of spasticity)³⁶, Ibuprofen (for treatment of pain, fever, rheumatoid arthritis and osteoarthritis)³⁷, and quinine in children³⁸ (for treatment of malaria), in the nasal delivery of selegiline hydrochloride (for treatment of Parkinson’s disease)³⁹ and opiorphin⁴⁰ (for treatment of acute and chronic pain), and vaginal delivery of itraconazole⁴¹ and clotrimazole⁴²(for treatment of vaginal candidiasis). No observable irritation to the mucosal membrane has been observed⁴³, hinting at the compatibility of P407-based formulations with the middle ear mucosa. Furthermore, delivery of OM treatments through a perforated tympanic membrane is particularly applicable to OM patients with recurrent episodes. A recent study showed 54.85% chronic OM cases are accompanied by tympanic membrane perforations⁴⁴, whereas among children with recurrent AOM 92% had tympanic membrane perforations⁴⁵. Therefore, the AgNPs reported here have the potential to enable a single-dose and sustained treatment for OM.

In this report, we obtained stable AgNPs colloidal solutions by reducing Ag⁺ in the presence of stabilizer polyvinylpyrrolidone. The as-synthesized particles were ~10 nm in diameter, as demonstrated using DLS and TEM. Upon successful demonstration of their antimicrobial efficacy in vitro using *S. pneumoniae*, NTHi, and *Streptococcus mutans* (*S. mutans*) and biocompatibility using human fibroblast and PC12 Adh cell line (a pheochromocytoma cell line used to test neurotoxicity), the particles were further incorporated in an 18% (w/v) P407 aqueous solution, yielding a hydrogel with reverse thermal gelation temperature at around 25°C. The hydrogel maintained high antimicrobial efficacy and biocompatibility. Therefore, the formulation reported here has the potential to eradicate bacterial pathogens of OM without antibiotics, which circumvents the systemic antibiotic exposure and associated harmful side effects caused by the current oral antibiotic therapy in OM treatment.

Experimental Section

Nanoparticles Synthesis

The stabilized polyvinylpyrrolidone-coated silver nanoparticles (AgNPs-PVP) were synthesized by a chemical reduction reaction as described in the literature⁴⁶. In short, silver nitrate (AgNO₃, 99.9% trace metals basis, Sigma, USA) and polyvinylpyrrolidone (PVP, MW 40000, Sigma, USA) were dissolved in deionized (DI) water separately and stirred on a magnetic stir plate until the solutions became homogeneous. Then AgNO₃ and PVP solutions were added together and stirred for 30 mins at 0°C, meantime sodium borohydride (NaBH₄, [?]^{98.0%}, Sigma, USA) was dissolved in DI water at 0degC in a separate flask. Next, the reducing agent solution was added dropwise into the AgNO₃-PVP mixture solution to reduce the Ag⁺-PVP to AgNPs-PVP. The color of the mixture solution became transparent bright yellow indicating formation of AgNPs-PVP. The final molarity concentration ratios of each component were AgNO₃:NaBH₄:PVP=2:1.4:1.

The AgNPs (AgNPs) was synthesized by chemical reduction reaction as a control to compare with the stability of AgNPs-PVP, using a protocol reported previously⁴⁷. In short, 0.25 mM AgNPs was made by adding 10 mL of 1.0 mM AgNO₃ dropwise to 30 mL of chilled 2.0 mM NaBH₄. The reaction mixture was stirred vigorously on a magnetic stir plate for 10 mins. Color of the mixture became clear yellow indicating the formation of AgNPs.

Characterization of AgNPs and AgNPs-PVP

Optical absorbance of AgNPs and AgNPs-PVP was monitored using a UV–Vis Spectrophotometer (Infinit(r) M1000 PRO) as a function of wavelength in the range from 300 to 500 nm. The incorporation of PVP was proven by a Bruker Vertex V80V Vacuum Fourier Transform Infrared Spectroscopy system (FTIR) in the range of 600-2100 cm⁻¹. The structures and sizes of nanoparticles were observed by 200 kV field emission Transmission Electron Microscopy (FEI F20 TEM/STEM) and Zetasizer (Nano 90) Dynamic Light Scattering (DLS). TEM showed images of particle size and shape on dried carbon-coated copper grid, and DLS gave the particle size in nanoparticle suspension solution.

Antibacterial Efficacy of AgNPs and AgNPs-PVP

Two gram-positive bacteria, *Streptococcus pneumoniae* (*S. pneumoniae*) and *Streptococcus mutans* (*S.*

mutans), and one gram-negative bacteria, non-typeable *Haemophilus influenzae* (NTHi), were chosen to test antibacterial effects of AgNPs-PVP. In short, *S. mutans* was cultured in Brain Heart Infusion (BHI) broth (BD Bioscience, USA), and both *S. pneumoniae* and NTHi were cultured in BHI medium with defibrinated horse blood and nicotinamide adenine dinucleotide (NADH) in a humidified 5% CO₂-containing balanced-air incubator at 37°C according to established protocols^{48–50}.

The suspension assay for estimation of the minimum inhibitory concentration (MIC) values was carried out to evaluate the antibacterial activity. The MIC values were determined on 96-well plates. Bacteria were cultured to serial dilutions of the AgNPs-PVP or AgNPs (3.125 μM, 6.25 μM, 12.5 μM, 25 μM, 50 μM, and 100 μM), and the end time points were determined when control group (bacteria only) grew to the stationary phase. Background from the nanoparticles alone was subtracted from the final reading. All assays were carried out in triplicates. All bacterial growth status were monitored by optical density at a wavelength of 600 nm (OD₆₀₀) using a UV-Vis Spectrophotometer (Infinite® M1000 PRO).

Biocompatibility Evaluation of AgNPs, PVP, and AgNPs-PVP

PC-12 cell line (ATCC CRL-1721.1) was cultured with F-12K medium supplemented (Corning, USA) with 2.5% fetal bovine serum (Gibco, USA), 15% horse serum (Gibco, USA) and 1% penicillin and streptomycin (Gibco, USA); and maintained in a humidified 5% CO₂-containing balanced-air incubator at 37°C.

PC-12 cells used in the assays were seeded in each well in the 96-well plates at the density of 1×10^4 cells per well overnight at 37 °C in a humidified 5% CO₂-containing atmosphere. After that, the media in each well was discarded. And cells were exposed to the AgNPs-PVP at concentrations of 3.125 μM, 6.25 μM, 12.5 μM, 25 μM, 50 μM, and 100 μM for 24h and 48h dissolved in fresh medium. Viability of PC-12 cells was evaluated using the CCK-8 kit for mammalian cells (Dojindo Molecular Technologies, Japan). The absorbance at 450 nm was measured after incubating cells with the CCK-8 assay for 1-2h. Empty wells with CCK-8 assay only were used as blanks and were subtracted from the final reading. Relative cell viability was calculated by normalizing the absorbance readings by that of untreated cells. All assays were carried out in quadruplicates.

Hydrogel Formation and Characterization

Hydrogel formulations were made by adding powdered poloxamer 407 (P407) to DI water and stirring the solution at 4°C until all powder was dissolved to form a clear solution. AgNPs-PVP was then added to the formulated P407 hydrogel solution and stirred until the solution became homogeneous. The hydrogel formulation was referred to as XμM[AgNPs-PVP]-18%[P407], where X indicates AgNPs-PVP concentration and 18% is weight per volume concentration of P407. Gelation temperature (T_{gel}), storage (G') and loss (G'') modulus were quantified using linear oscillatory shear rheology measurements (1 rads⁻¹, 1% strain, and 1°C/min) by TA Instruments DHR3 Rheometer. T_{gel} is taken as the temperature when the G' became 2KPa larger than the G'' . The changes of G' and G'' were recorded in the temperature range of 20°C to 40°C.

In Vitro Release Kinetics of Hydrogel Formulations

The release of AgNPs-PVP from the hydrogel formulations was detected using a similar diffusion system as described in the literature⁵¹. Transwell membrane inserts (3-μm pore size and 1.1 cm² area; Costar, USA) and 24-well plates were used as the donor and acceptor cells, respectively. A 200 μL aliquot of the formulation containing 18% P407 and 50 or 100 μM AgNPs-PVP was pipetted onto the prewarmed inserts' membrane to get a solid-like hydrogel. Transwell inserts with solid-like hydrogel were placed into the 24-well plates with each well containing 1000 μL prewarmed phosphate-buffered saline (PBS). Then the plates were incubated at 37°C. The 1000 μL aliquots of the PBS were collected at each time point (0.5, 1, 3, 6, 24, and 48 hours), and the inserts were moved to a new well with 1000 μL fresh and prewarmed PBS. Collected aliquots were analyzed with UV-Vis Spectrophotometer; a standard curve was made to determine the AgNPs-PVP concentrations. Experiments were performed in triplicates.

Biocompatibility Evaluation of Hydrogel Formulations

The primary dermal fibroblast cell line (ATCC PCS-201-012) was cultured using the Fibroblast Growth Kit-Low Serum (ATCC PCS-201-041) in a humidified 5% CO₂-containing balanced-air incubator at 37°C.

Fibroblast cells used in the assays were seeded in each well in the 24-well plates at the density of 4×10⁴ cells per well overnight at 37 °C in a humidified 5% CO₂-containing atmosphere. After that, the media in each well was discarded. And cells were exposed to the AgNPs-PVP at concentrations of 3.125 μM, 6.25 μM, 12.5 μM, 25 μM, 50 μM, and 100 μM for 24h dissolved in fresh medium. Viability of fibroblast cells was evaluated using a LIVE/DEAD cytotoxicity kit (Invitrogen, USA) which was diluted 1000-fold into PBS. The live/dead image was obtained by Confocal (Zeiss LSM800) after incubating cells with the LIVE/DEAD staining assay for about 30 mins. Untreated cells with the assay were used as control. Relative cell viability was calculated by normalizing the reading of number of live cells by that of untreated cells via ImageJ. All assays were carried out in quadruplicates.

Antibacterial Test of Hydrogel Formulations

500 μL of 100μM[AgNPs-PVP]-18%[P407] was pipetted into a 5 mL round bottom tube and stored at 37°C until the formulations became solid-like gel. Next, the 500 μL of prewarmed bacterial broth was added into the tube. The tube was subsequently incubated at 37 °C in a humidified 5% CO₂-containing atmosphere for 24 hours. At the end of the incubation, 100 μL suspension was spread onto appropriate agar plates following the spread plates technology and incubated for 24 hours before colony forming units were counted.

Results and Discussion

Synthesis and Characterization of AgNPs-PVP and Unprotected AgNPs

AgNPs were synthesized via the commonly adopted approach of reducing silver ions (Ag⁺) in the presence of a polymeric stabilizer⁵². Sodium borohydride (BH₄⁻) was used as the reducing agent⁵³ because of its rapid reaction with Ag⁺ and room-temperature reaction conditions. Ag⁺ and BH₄⁻ quickly reacted to produce AgNPs following the equation below⁴⁶:



As-synthesized AgNPs are prone to aggregation, driven by changes in pair potential as a result of the spontaneous hydrolysis of BH₄⁻ and production of sodium hydroxide and orthoborate ([BO₃]³⁻)^{46,54}. To prevent the aggregation of AgNPs and control their sizes, PVP was used due to its strong interaction with Ag⁺, which slowed down the growth of silver grains. And the distance between the resulting silver particles is larger than that of the silver particles without PVP⁵⁵). Compared to other stabilizers, such as polyvinyl alcohol (PVA)⁵⁶, PVP demonstrated greater size-regulating capability, likely due to its stronger affinity to Ag⁺ (e.g., the hydroxyl groups in PVA led to weaker interaction than that of Ag⁺-PVP⁵⁷ and cellulose⁵⁸ merely acted as a matrix for controlled diffusion of Ag⁺⁵⁹). The synthesis followed an established protocol⁴⁶, where 3.75 mL of an aqueous solution of PVP (1 mM) was added to 7.5 mL of an aqueous solution of AgNO₃ (1 mM); and 18.75 mL of an aqueous solution of NaBH₄ (0.2 mM) was added dropwise to obtain AgNPs-PVP with the final concentration of 0.25 mM. The Ag:PVP:NaBH₄ ratio of 2:1:1.4 was chosen based on the good stability of as-synthesized AgNPs-PVP in previous reports⁴⁶. FTIR spectra of PVP and AgNPs-PVP both showed a pronounced peak at 1640 cm⁻¹, indicating C=O stretching and thus presence of PVP. Furthermore, the FTIR spectra of unprotected AgNPs and AgNPs-PVP both showed a peak at 1060 cm⁻¹, representing O-H vibration and presence of AgNPs. Therefore, the spectrum of AgNPs-PVP indicated that the characterizations of both AgNPs and PVP were fully retained in AgNPs-PVP.

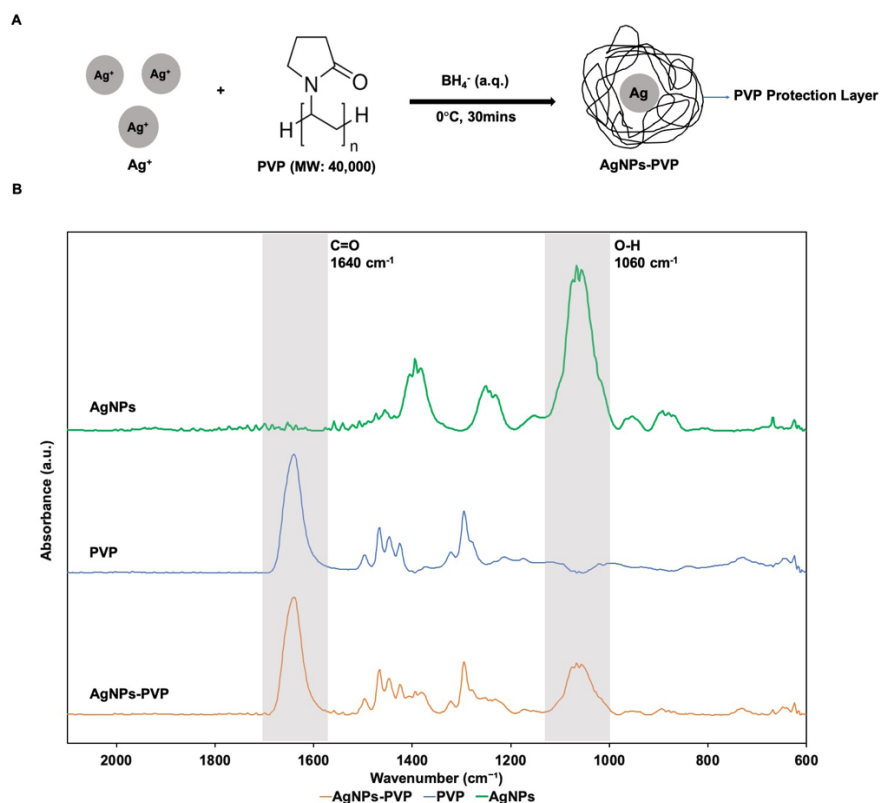


Figure 1. Synthesis and FTIR Characterization of AgNPs-PVP. **A)** Aqueous solutions of $AgNO_3$ (1 mM; 7.5 mL) and PVP (1 mM; 3.75 mL) were combined and kept at $0^\circ C$ for 30 minutes to ensure the mixture was homogeneous and temperature was cool enough for addition of $NaBH_4$ ($NaBH_4$ reacted violently and quickly with water at room temperature) and prevention of aggregation (the nanoparticles were grown more rapidly at room temperature), where addition of an aqueous solution of $NaBH_4$ to the final concentration of 0.175 mM initiated formation of AgNPs-PVP. **B)** FTIR spectra of AgNPs, PVP, and AgNPs-PVP, demonstrating AgNPs-PVP retained peaks from both of AgNPs (O-H at around $1060\ cm^{-1}$) and PVP (C=O at around $1640\ cm^{-1}$).

Sizes of the AgNPs-PVP and unprotected AgNPs were characterized using DLS and TEM. For an aqueous solution of AgNPs-PVP (0.25 mM; AgNPs:PVP=2:1) (Figure 2A), DLS indicated a narrow range of size distribution, with an average diameter of $9.23 \pm 2.03\ nm$ and polydispersity index (PDI) of 0.149. In contrast, DLS captured a much broader size distribution for an aqueous solution of unprotected AgNPs (0.25 mM) due to aggregation, with an average diameter of $31.55 \pm 7.9\ nm$ and PDI of 0.336. TEM images further provided direct evidence of the effect of PVP on preventing the aggregation of AgNPs (Figure 2B). While AgNPs-PVP demonstrated a spherical morphology with an average diameter of $10.54 \pm 3.11\ nm$ (Figure 2B and 2D), substantial aggregation was captured for unprotected AgNPs (Figure 2B). The characteristic length of the aggregates was calculated to be $25.82 \pm 11.98\ nm$ (Figure 2C), obtained by processing TEM images using ImageJ. The fact that DLS measured an average diameter greater than that captured by TEM is well documented in the literature^{60,61}. It has been attributed to the hydrodynamic diameter (as measured by DLS) being greater than the projected area diameter (as captured by TEM), due to a solvent layer surrounding a colloid that are subject to the particle Brownian motion.

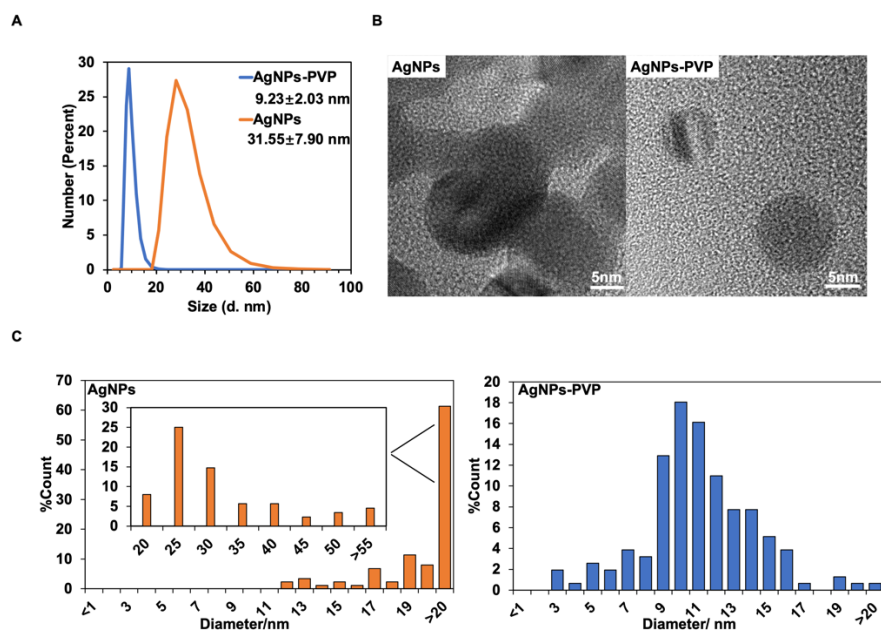


Figure 2. DLS and TEM analyses of particle sizes . A) DLS indicated a narrow size distribution for AgNPs-PVP, with an average diameter of 9.23 ± 2.03 nm and a PDI of 0.149; whereas unprotected AgNPs demonstrated an average diameter of 31.55 ± 7.9 nm with PDI of 0.336. **B)** TEM images of unprotected AgNPs and AgNPs-PVP, showing aggregates for the former and regular spherical morphology for the latter. **C)** Particle size distributions of unprotected AgNPs (25.82 ± 11.98 nm) and AgNPs-PVP (10.54 ± 3.11 nm) obtained by analyzing TEM images ($n = 3$ for each case) using ImageJ. The inset demonstrates the detailed size distribution for unprotected AgNPs with characteristic lengths > 20 nm. Data are mean \pm SD.

Upon dispersion in water at the concentration of 0.25 mM, AgNPs-PVP formed a stable colloidal solution (Figure 3B), which remained unchanged after 7 days of storage under ambient conditions. The solution exhibited a maximum absorption at 404 nm, as characterized using UV-vis spectrophotometry (Figure 3B, corresponding to the bright yellow color), which also remained unchanged after the 7-day storage. Although a freshly made aqueous solution of unprotected AgNPs (0.25 mM) exhibited a similar color as that of AgNPs-PVP, the absorption peaks at 375 nm and 425 nm hinted at the polydispersed particle sizes due to aggregation. After 7 days of storage, the solution demonstrated a dark grey color, with no discernable UV-vis absorption (Figure 3A), indicating instability of the solution. The superior stability of AgNPs-PVP solutions likely led to their greater antimicrobial efficacy against OM pathogens, as described below.

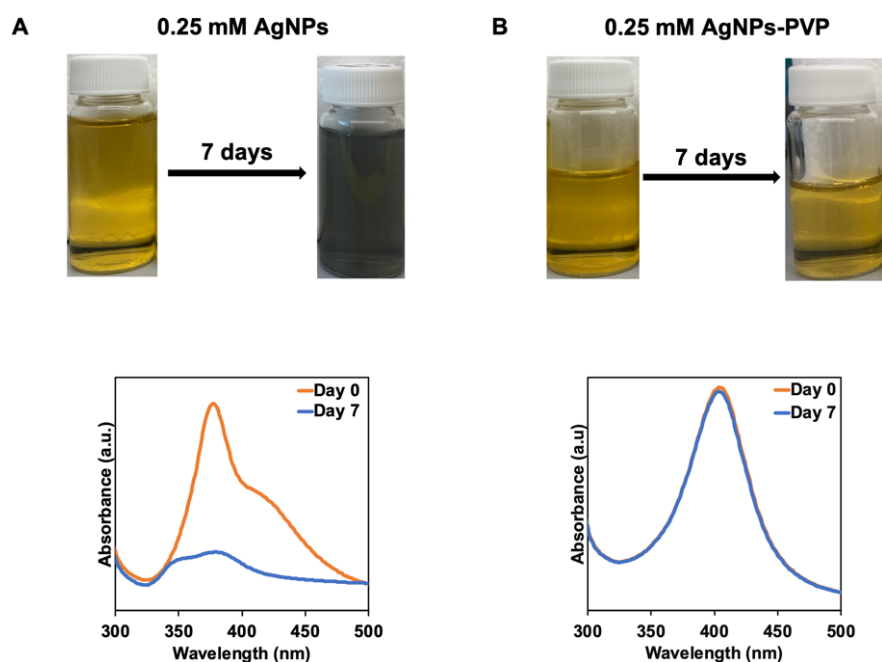


Figure 3. Greater stability of an aqueous solution of AgNPs-PVP (0.25 mM) than unprotected AgNPs (0.25 mM), demonstrated via visual inspection and UV-vis spectrophotometry . A) Photographs of an aqueous solution of unprotected AgNPs (0.25 mM) that was freshly made and after 7 days of storage under ambient conditions, along with the UV-vis spectra under each condition. **B)** Photographs of an aqueous solution of AgNPs-PVP that was freshly made and after 7 days of storage under ambient conditions, along with the UV-vis spectra under each condition. The maximum absorption at 404 nm remained throughout the storage.

Antibacterial Efficacy of AgNPs-PVP and Unprotected AgNPs

As discussed previously, *S. pneumoniae* and NTHi are the two most common bacteria pathogens causing OM, accounting for 58% of the total OM episodes in the US^{4,5}. The antibacterial efficacy of AgNPs-PVP and unprotected AgNPs was thus tested using these two pathogens. The minimum inhibitory concentration (MIC) and half maximal inhibitory concentration (IC₅₀) were used to quantify the antibacterial efficacy. MIC was obtained via broth microdilution assay, where MIC corresponds to the lowest concentration of antimicrobials that prevented bacterial growth. To better characterize the affected bacterial growth before complete eradication (i.e., MIC) was achieved, IC₅₀ was calculated, defined as the concentration of antimicrobials that led to a stationary OD₆₀₀ that was half of that without antimicrobials. For antimicrobials with the same MIC, lower IC₅₀ indicates higher antimicrobial effect.

The antimicrobial efficacy of AgNPs against NTHi showed an average IC₅₀ of 28.72 μ M (~4.88 μ g/mL) and an average MIC of 50 μ M (~8.5 μ g/mL) (Figure 4A). The average values of IC₅₀ and MIC were much reduced in the presence of PVP, which became 9.45 μ M (~1.61 μ g/mL) and 12.5 μ M (~2.13 μ g/mL) respectively (Figure 4A). The greater antimicrobial efficacy of AgNPs-PVP than unprotected AgNPs was likely a result of the stabilized particulates (Figure 3) with greater surface-to-volume ratio than aggregates that led to enhanced interactions with pathogens.

The antibacterial efficacy of AgNPs-PVP was comparable to tradition antibiotics against NTHi, such as Amoxicillin (with MIC of 0.5 - 2 μ g/mL), Clarithromycin (with MIC of 2 - 8 μ g/mL), and Azithromycin (with MIC of 0.25 - 2 μ g/mL)⁶². Contrary to those small-molecule antibiotics, efficacy of AgNPs and AgNPs-PVP against *S. pneumoniae* was better than that against NTHi (Figure 4B), with IC₅₀ values of 17.88 μ M (~2.99 μ g/mL) and 4.14 μ M (~0.70 μ g/mL) for AgNPs and AgNPs-PVP respective and MIC

values of 25 μM ($\sim 4.18 \mu\text{g/mL}$) and 6.25 μM ($\sim 1.04 \mu\text{g/mL}$) for AgNPs and AgNPs-PVP respective. The stronger antimicrobial effects of AgNPs and AgNPs-PVP against *S. pneumoniae* than that against NTHi could be due to their gram types or the known production of H_2O_2 by *S. pneumoniae* (at levels around 0.1 – 0.71 mM as a mechanism for competitive survival during coinfections)⁶³. To better understand this differential efficacy of AgNPs-PVP, *Streptococcus mutans* (*S. mutans*), a gram-positive pathogen (same as *S. pneumoniae*) with much lower activity of H_2O_2 production (at levels around 0 - 0.06 mM^{64,65}) was tested.

S. mutans is one of the microorganisms inhabiting the oral cavity, which has been studied for its etiology of dental caries and infective endocarditis⁶⁶. Interestingly, the colonization of *S. mutans* in mouth has been shown to be correlated with the colonization of *S. pneumoniae* in the nasopharynx⁶⁷, thus making *S. mutans* a pathogen of interest for OM treatment. Indeed, the MIC values of AgNPs and AgNPs-PVP against *S. mutans* were 50 μM ($\sim 8.35 \mu\text{g/mL}$) and 12.5 μM ($\sim 2.09 \mu\text{g/mL}$) respectively, which were comparable to NTHi and greater than *S. pneumoniae* (Figure 4C). Similarly, the IC_{50} value of AgNPs and AgNPs-PVP against *S. mutans* were 32.03 μM ($\sim 5.35 \mu\text{g/mL}$) comparable to that of NTHi. The IC_{50} value of AgNPs-PVP, 4.87 μM ($\sim 0.81 \mu\text{g/mL}$), was smaller than that of NTHi (9.45 μM ($\sim 1.58 \mu\text{g/mL}$)) and close to that of *S. pneumoniae* (4.14 μM ($\sim 0.70 \mu\text{g/mL}$)), which could be explained by the bacteriostatic effect of low levels of H_2O_2 on *S. mutans*⁶⁸. Taken together, the MIC and IC_{50} values of AgNPs and AgNPs-PVP against *S. mutans* confirmed that their greater efficacy against *S. pneumoniae* was likely a result of the H_2O_2 -producing capability and not gram types, as gram-positive *S. mutans* and gram-negative NTHi demonstrated comparable values.

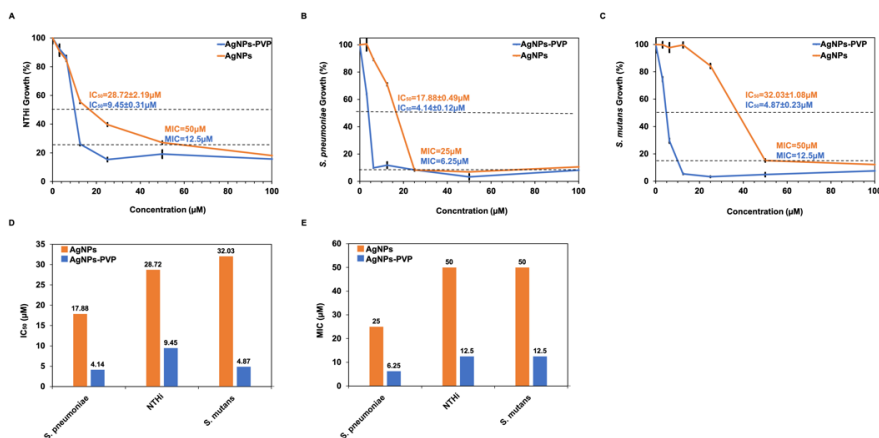


Figure 4. Antibacterial effect of unprotected AgNPs and AgNPs-PVP. A-C) Growth of NTHi (A), *S. pneumoniae* (B), and *S. mutans* (C) after 12 hours of incubation without or with varying concentrations of AgNPs and AgNPs-PVP, normalized by the growth without antimicrobials (i.e., 100% growth represents the growth of bacteria without AgNPs or AgNPs-PVP). MIC and IC_{50} are indicated with dashed lines. Data are mean \pm SD. D-E) Summary of IC_{50} (D) and MIC (E) values of AgNPs and AgNPs-PVP against NTHi, *S. pneumoniae* and *S. mutans*. n=3 for each group.

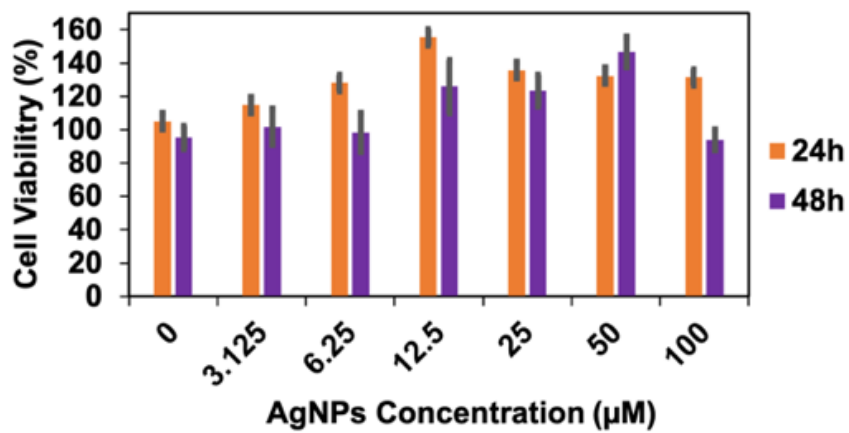
Cytotoxicity of AgNPs-PVP and Unprotected AgNPs

Cytotoxicity of AgNPs and AgNPs-PVP was evaluated by applying the CCK-8 assay on the PC12 Adh cell line. The percentage of cell viability was assessed at different concentrations of AgNPs, PVP, and AgNPs-PVP, respectively (Figure 5).

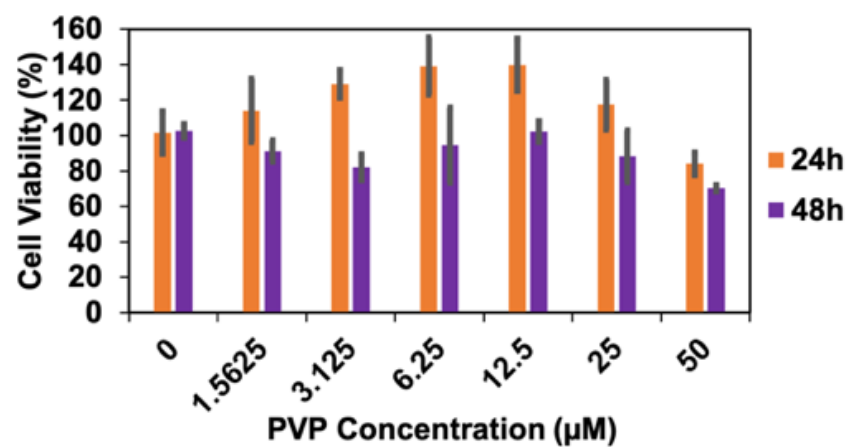
AgNPs showed negligible cytotoxicity in the concentration range of 0 – 100 μM (far exceeded the MIC for all three pathogens tested) at 24 and 48 hours (Figure 5A). Cytotoxicity of PVP alone was assessed in the concentration range of 0 – 50 μM (Figure 5B), corresponding to the range used in the AgNPs-PVP formulations (AgNPs-PVP formulations were made with a 2:1 molar ratio of AgNPs and PVP). PVP also demonstrated minimal cytotoxicity, consistent with the biocompatibility reported in the literature⁶⁹. All

concentrations of AgNPs-PVP formulations demonstrated virtually unchanged cell viability (Figure 5C), indicating excellent biocompatibility. At 48 hours, mild cytotoxicity was observed for AgNPs-PVP at the concentrations of 50 μM and 100 μM (representing the concentrations of AgNPs), with cell viability values of 80% and 20% respectively (Figure 5C). Nevertheless, the AgNPs-PVP formulation caused no observable cytotoxicity at concentrations at or below the MICs (i.e., 12.5 μM for NTHi and *S. mutans* and 6.25 μM for *S. pneumoniae*) at both 24 and 48 hours and the formulation was thus considered safe under effective concentrations.

A



B



C

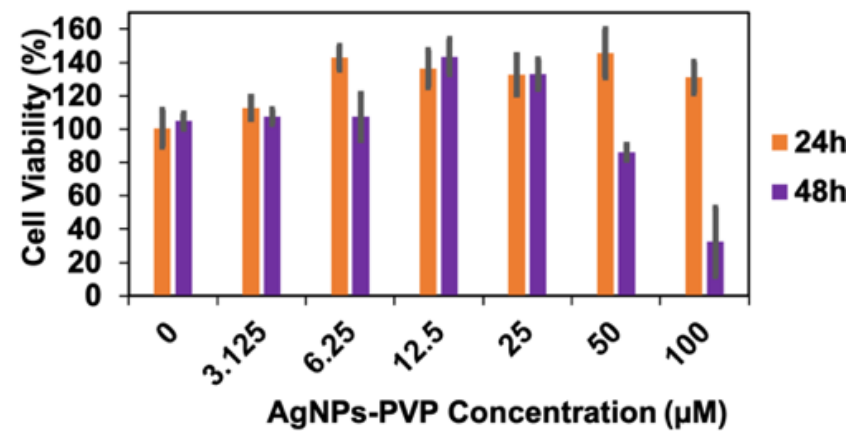


Figure 5. Cytotoxicity of AgNPs, PVP, and AgNPs-PVP.A-C) Cell viability of PC-12 after incubating with different concentrations of AgNPs, PVP, and AgNPs-PVP, at 24 and 48 hours. Culture of PC-12 without any exposure to AgNPs, PVP, or AgNPs-PVP was considered 100% cell viability. Error bars represent standard deviations. n = 4 for each group.

Formulation and Rheology of the Antimicrobial and Temperature-Responsive Hydrogel Delivery System

AgNPs-PVP was chosen to formulate the hydrogel delivery system due to its superior antimicrobial efficacy compared to unprotected AgNPs. AgNPs-PVP was added to an 18%(w/v) P407 aqueous solution to formulate the antimicrobial and temperature-responsive hydrogel, with concentration of the AgNPs-PVP (Ag:PVP ratio of 2:1) in the hydrogel varied in the range of 0-100 μ M. The resulting formulation was referred to as X μ M[AgNPs-PVP]-18%[P407], where X indicated the concentration of Ag (Figure 6A).

As discussed previously, P407 was used here due to its reverse thermal gelation properties, i.e., the AgNPs-PVP-containing formulation could flow readily into the middle ear space during administration, and then gel promptly at 37°C to ensure sustained antimicrobial effect. The concentration of P407, i.e., 18% (w/v), was selected based on our prior experience, which led to a gelation temperature close to 37°C and sufficient gel strength to sustain drug delivery over the 7 – 10 day-course of treatment⁵¹.

Linear oscillatory shear rheology of the AgNPs-PVP-containing hydrogel formulations demonstrated that introduction of the nanotherapeutics at concentrations at or below 100 μ M did not jeopardize the desirable reverse thermal gelation. For each formulation, storage (G') and loss (G'') moduli were quantified in the temperature range of 20 – 40°C; and gelation (i.e., the transition from a liquid formulation to a solid gel) was defined as the point where G' was greater than G'' by 2kPa. Without the nanotherapeutics, the formulation containing 18%[P407] had a gelation temperature of 25 °C, and G' and G'' of 12.27 +- 0.42 kPa and 4.22 +- 0.21 kPa at 37°C (Figure 6B). At the AgNPs-PVP concentration of 50 μ M, the hydrogel formulation demonstrated virtually unchanged gelation temperature of 24 °C, and G' and G'' of 12.29 +- 0.19 kPa and 4.63 +- 0.14 kPa respectively at 37°C (Figure 6C). With 100 μ M AgNPs-PVP, the gelation temperature remained at 24 °C, with G' and G'' values increased to 14.41 +- 1.91 kPa and 6.07 +- 0.50 kPa at 37°C (Figure 6D), which was likely a result of the entanglement between PVP and P407 chains. Gelation did not occur for the formulation of 200 μ M[AgNPs-PVP]-18%[P407] and G' was reduced to 5.29 \pm 0.66 kPa, merely half of that of 18%[P407] (Figure 6E). This could be attributed to the inability for P407 chains to form micelles and/or for micelles to pack into a solid gel due to the substantial presence of PVP chains. Values of the gelation temperatures and storage/loss moduli were summarized in a table (Figure 6F).

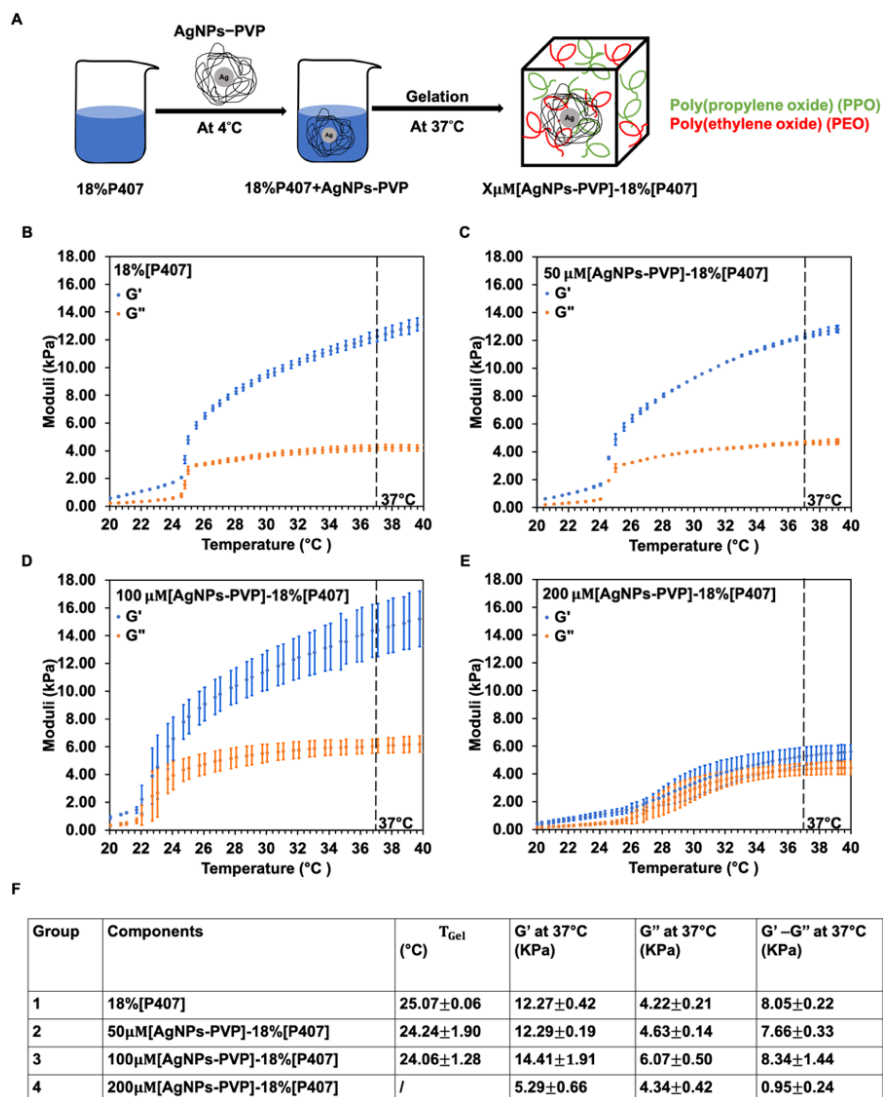
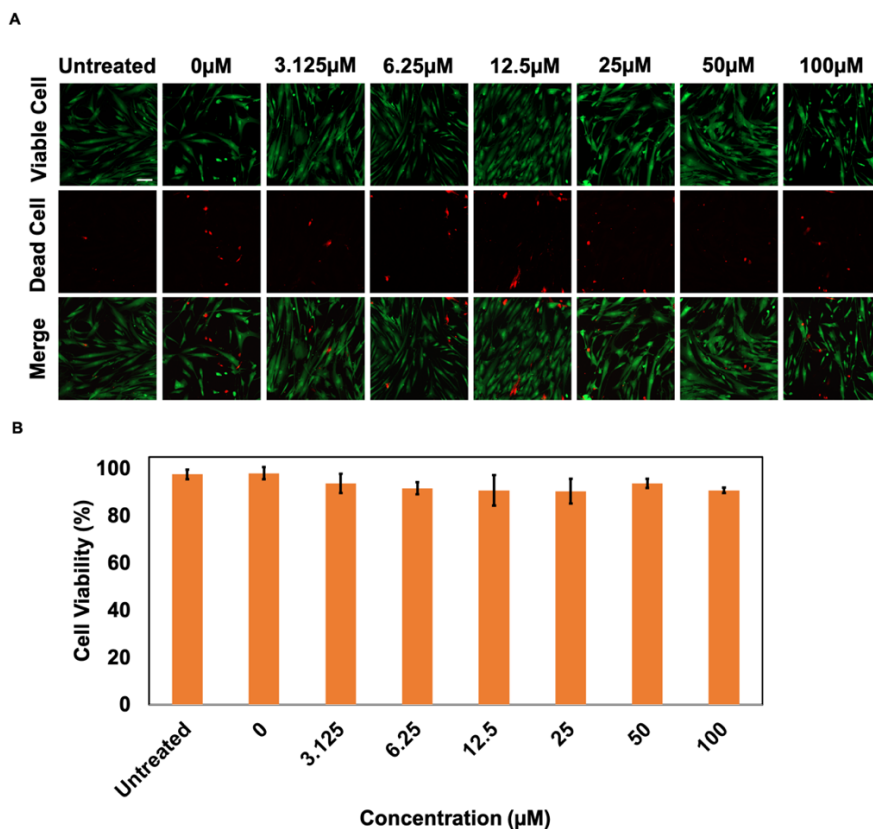


Figure 6. Formulation and Rheology of the Antimicrobial and Temperature-Responsive Hydrogel Delivery System . **A)** Formulation of the hydrogels. AgNPs-PVP was introduced to an 18%(w/v) aqueous solution of P407 to the final concentrations of 50 μ M, 100 μ M, and 200 μ M respectively. The formulations were thereafter referred to as $X\mu$ M[AgNPs-PVP]-18% [P407], where X indicates the concentration of Ag. **B-E)** Linear oscillatory shear rheology of the formulations containing 18% [P407] (**B**), 50 μ M[AgNPs-PVP]-18% [P407] (**C**), 100 μ M[AgNPs-PVP]-18% [P407] (**D**), and 200 μ M[AgNPs-PVP]-18% [P407] (**E**), with dashed lines highlighting the storage modulus G' and loss modulus G'' at 37°C. **F)** Summary of gelation temperatures and values of G' and G'' at 37°C, for the four aforementioned formulations. Data are mean \pm SD. n = 3 for each group.

Cytotoxicity of the Hydrogel Formulations

Cytotoxicity of $X\mu$ M[AgNPs-PVP]-18% [P407] with Ag concentration ranging from 0 μ M to 100 μ M was evaluated using human dermal fibroblast (hFBs), a common cell line used to assess cytotoxicity of topical formulations. All formulations of $X\mu$ M[AgNPs-PVP]-18% [P407] showed negligible cytotoxicity (Figure 7A), indicating excellent biocompatibility. The cell viability results were further quantified by counting live cell numbers using ImageJ, demonstrating >90% viability for all hydrogel formulations tested. Cytotoxicity was

markedly improved for 50 μ M[AgNPs-PVP]-18%P407 and 100 μ M[AgNPs-PVP]-18%P407 compared to the aqueous solutions of 50 μ M and 100 μ M AgNPs-PVP (Figure 5C). This phenomenon could be attributed to the sustained release and thus controlled dosing of AgNPs-PVP from the hydrogel formulations, effectively reducing the concentration of AgNPs-PVP to which hFBs cells were exposed. The formulations of 50 μ M and 100 μ M[AgNPs-PVP]-18%P407 were selected for further assessment of in vitro release studies given their excellent biocompatibility.

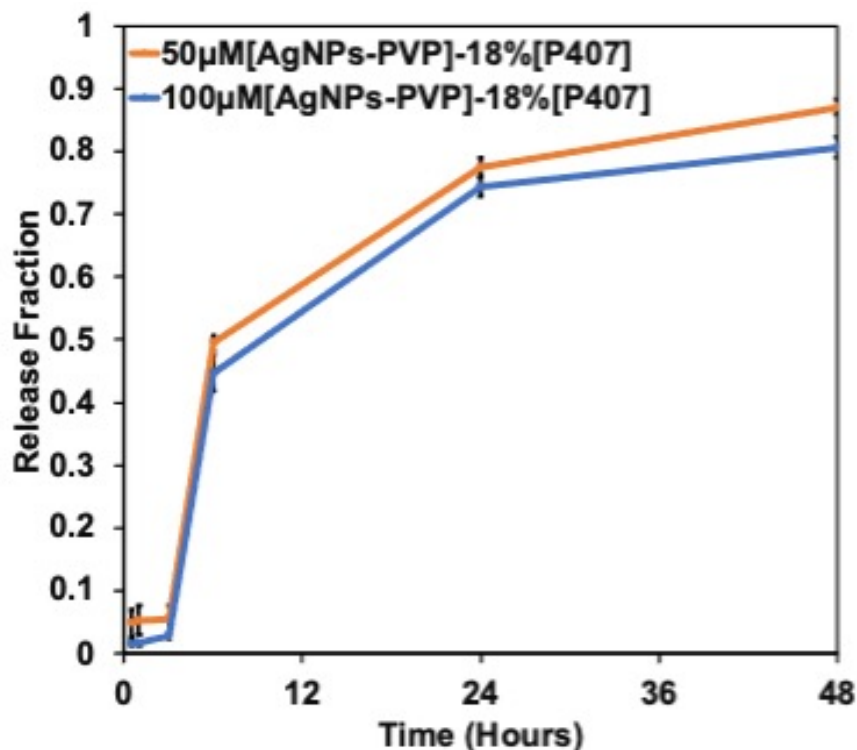


Φιγυρε 7. Τοξικιτιψ εαλατιον οφ φορμουλατιονς Ξ μ M[ΑγΝΠΙσ-Π'Π]-18%[Π407]. **A)** Confocal images of hFBs after incubating with X μ M[AgNPs-PVP]-18%P407 (X = 0, 3.125, 6.25, 12.5, 25, 50, or 100) for 24 hours, followed by LIVE/DEAD staining assay. Scale bar represents 100 μ m. **B)** The percentage cell viability obtained by counting the number of cells in the confocal images (similar to A, n = 4 for each group) using ImageJ. Data represents mean \pm SD.

In vitro Release of AgNPs-PVP from the Hydrogel Formulations with Reverse Thermal Gelation

The cumulative release of AgNPs-PVP was studied by quantifying the in vitro diffusion of Ag from hydrogel formulations placed in a Transwell[®]. Effect of initial drug loading amount on release kinetics of the hydrogel formulations was investigated using two hydrogel formulations, 50 μ M[AgNPs-PVP]-18%P407 and 100 μ M[AgNPs-PVP]-18%P407. Consistent with previous reports^{51,70}, lower initial drug loading amount resulted in slightly greater cumulative release fraction by the end of the 48 hour testing period (Figure 8). At 3 hours, the two formulations had similarly low release fractions, i.e., 5.38 ± 2.32 % for 50 μ M[AgNPs-PVP]-18%P407 and 2.79 ± 0.40 % for 100 μ M[AgNPs-PVP]-18%P407. The total amounts of Ag released from the two formulations were comparable. At 6 hours, 49.49 ± 1.24 % was released from 50 μ M[AgNPs-PVP]-18%P407 and 44.64 ± 2.94 % from 100 μ M[AgNPs-PVP]-18%P407, where the amount of Ag released from

the latter exceeded that of the former by nearly two-fold, implying that the release of Ag was dominated by passive diffusion. Similar observations were made at 24 and 48 hours, i.e., 50 μ M[AgNPs-PVP]-18%[P407] achieved cumulative release fractions of 77.41 ± 1.60 % and 87.03 ± 1.25 % respectively, and 100 μ M[AgNPs-PVP]-18%[P407] achieved 74.37 ± 1.56 %, and 80.61 ± 1.65 % respectively. The cumulative release fractions of 100 μ M[AgNPs-PVP]-18%[P407] were slightly less than two-fold that of 50 μ M[AgNPs-PVP]-18%[P407] at 6, 24, and 28 hours, which was likely a result of the aforementioned entanglement between PVP and P407 chains that increased physical cross-linking and reduced rate of passive diffusion.



Φιγυρε 8. Ομυλατιε ιν ιτρο ρελεασε οφ Αγ φρομ 50 μ M[ΑγΝΠσ-Π΄Π]-18%[Π407] ανδ 100 μ M[ΑγΝΠσ-Π΄Π]-18%[Π407]. n = 3 for each group. Data were mean \pm SD.

Antibacterial Efficacy of the AgNPs-PVP-Containing Hydrogel

Using the formulation containing the highest concentration of AgNPs-PVP while still maintaining reverse thermal gelation, i.e., 100 μ M[AgNPs-PVP]-18%[P407], antimicrobial efficacy was examined. As discussed previously, *S. pneumoniae* and NTHi, the two main pathogens causing OM^{4,5}, were used.

To mimic the environment of an auditory bullae during an active episode of OM, which has the volume of 1.52 ± 0.26 mL (mean \pm SD)⁷¹, 500 μ L hydrogel formulation was applied to 500 μ L bacteria broth and incubated for 24 hours. The antibacterial activity of hydrogel formulations was assessed by counting the colony-forming unites (CFU) at the end of the 24-hour incubation (Figure 9). While countless colonies of *S. pneumoniae* and NTHi were observed on the agars that were untreated or treated with 18%[P407], 100 μ M[AgNPs-PVP]-18%[P407] achieved complete eradication of both pathogens, demonstrating the potential of this local treatment to cure OM with high bacterial counts.



Figure 9. Antibacterial efficacy of the hydrogel delivery system tested using *Streptococcus pneumoniae* and NTHi. The 100µM[AgNPs-PVP]-18%[P407] formulation (500 µL) was stored at 37°C until it became a solid-like gel; prewarmed bacterial broth (500 µL) was subsequently added to the hydrogel. The tube was then incubated at 37°C for 24 hours, by the end of which, 100 µL of the culture was applied on agar plates and incubated for 24 hours. The hydrogel formulation, 100µM[AgNPs-PVP]-18%[P407] completely eradicated both *S. pneumoniae* and NTHi.

Conclusion

In summary, we designed a hydrogel formulation (100µM[AgNPs-PVP]-18%[P407]), which achieved complete eradication of the two most common bacterial OM pathogens, i.e., *S. pneumoniae* and NTHi in vitro without causing cytotoxicity. The AgNPs-PVP was synthesized via a chemical reduction reaction using NaBH₄ as the reducing agent and PVP as the stabilizer. The as-synthesized AgNPs-PVP demonstrated a narrow size distribution (~10 nm), which led to their effective eradication of the bacterial OM pathogens at MIC values of 6.25 µM (~1.04 µg/mL) for *S. pneumoniae* and 12.5 µM (~2.13 µg/mL) for NTHi. To realize the local and sustained delivery of the AgNPs-PVP, a hydrogel with reverse thermal gelation properties was formulated, promising a delivery system with ease of administration through (perforated) tympanic membranes and sustained presence in the auditory bullae. Gelation temperature of the final hydrogel formulation, 100µM[AgNPs-PVP]-18%[P407], was measured to be 24.06 ± 1.28 °C using linear oscillatory shear rheology. The antimicrobials released from 100µM[AgNPs-PVP]-18%[P407] eradicated the two aforementioned OM pathogens without triggering cytotoxicity. This was the first time that AgNPs were used against OM pathogens, and the hydrogel formulation thus points to an effective and biocompatible solution to treat OM while circumventing the health concerns associated with systemic antibiotic exposure.

ASSOCIATED CONTENT

Author Contributions

X.M. and J.L. contributed equally to this paper.

Funding Sources

National Institutes of Health, National Institute on Deafness and Other Communication Disorders (NIHDC016644)

Notes

The authors declare no competing financial interest.

ACKNOWLEDGMENT

The authors acknowledge the National Institutes of Health - National Institute on Deafness and Other Communication Disorders for support (NIHDC016644 to R.Y.). Analytical methods involved use of the Cornell Center for Materials Research (CCMR) Shared Facilities which are supported through the NSF MRSEC program (DMR-1719875). We thank J. Grazul for support TEM preparation.

Reference

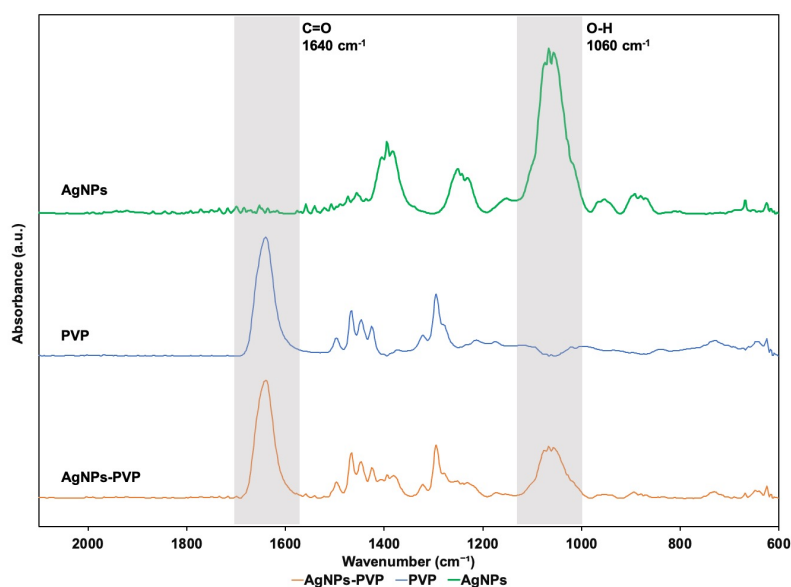
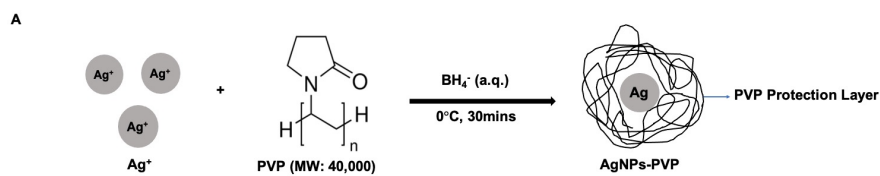
1. Paul CR, Moreno MA. Acute Otitis Media. *JAMA Pediatr* . 2020;174(3):308. doi:10.1001/jamapediatrics.2019.5664
2. Teele DW, Klein JO, Rosner B. Epidemiology of Otitis Media during The First Seven Years of Life in Children in Greater Boston: A Prospective, Cohort Study. *J Infect Dis* . 1989;160(1):83-94. doi:10.1093/infdis/160.1.83
3. Shaffer AD, Ford MD, Choi SS, Jabbour N. The impact of timing of tympanostomy tube placement on sequelae in children with cleft palate. *Cleft Palate-Craniofacial J* . 2019;56(6):720-728. doi:10.1177/1055665618809228
4. Ruohola A, Meurman O, Nikkari S, et al. Microbiology of acute otitis media in children with tympanostomy tubes: Prevalences of bacteria and viruses. *Clin Infect Dis* . 2006;43(11):1417-1422. doi:10.1086/509332
5. Bluestone CD, Stephenson JS, Martin LM. Ten-year review of otitis media pathogens. *Pediatr Infect Dis J* . 1992;11(8):S7-11.
6. Schilder AGM, Chonmaitree T, Cripps AW, et al. Otitis media. *Nat Rev Dis Prim* . 2016;2:1-19. doi:10.1038/nrdp.2016.63
7. Ayukekbong JA, Ntemgwa M, Atabe AN. The threat of antimicrobial resistance in developing countries: Causes and control strategies. *Antimicrob Resist Infect Control* . 2017;6(1):1-8. doi:10.1186/s13756-017-0208-x
8. Van Dyke MK, Pirçon JY, Cohen R, et al. Etiology of acute otitis media in children less than 5 years of age: A pooled analysis of 10 similarly designed observational studies. *Pediatr Infect Dis J* . 2017;36(3):274-281. doi:10.1097/INF.0000000000001420
9. Littorin N, Ahl J, Uddén F, Resman F, Riesbeck K. Reduction of Streptococcus pneumoniae in upper respiratory tract cultures and a decreased incidence of related acute otitis media following introduction of childhood pneumococcal conjugate vaccines in a Swedish county. *BMC Infect Dis* . 2016;16(1):1-8. doi:10.1186/s12879-016-1750-5
10. Davies TA, Yee YC, Goldschmidt R, Bush K, Sahm DF, Evangelista A. Infrequent occurrence of single mutations in topoisomerase IV and DNA gyrase genes among US levofloxacin-susceptible clinical isolates of Streptococcus pneumoniae from nine institutions (1999-2003). *J Antimicrob Chemother* . 2006;57(3):437-442. doi:10.1093/jac/dki487
11. DK Chen AM. Decreased Susceptibility of Streptococcus Pneumoniae. *Nejm* . Published online 1999:233-239.
12. Arens A. Treatment of acute otitis media in children under 2 years of age. *J Emerg Med* . 2011;40(6):722-723. doi:10.1016/j.jemermed.2011.04.009
13. Oves M, Aslam M, Rauf MA, et al. Antimicrobial and anticancer activities of silver nanoparticles synthesized from the root hair extract of Phoenix dactylifera. *Mater Sci Eng C* . 2018;89(March):429-443. doi:10.1016/j.msec.2018.03.035

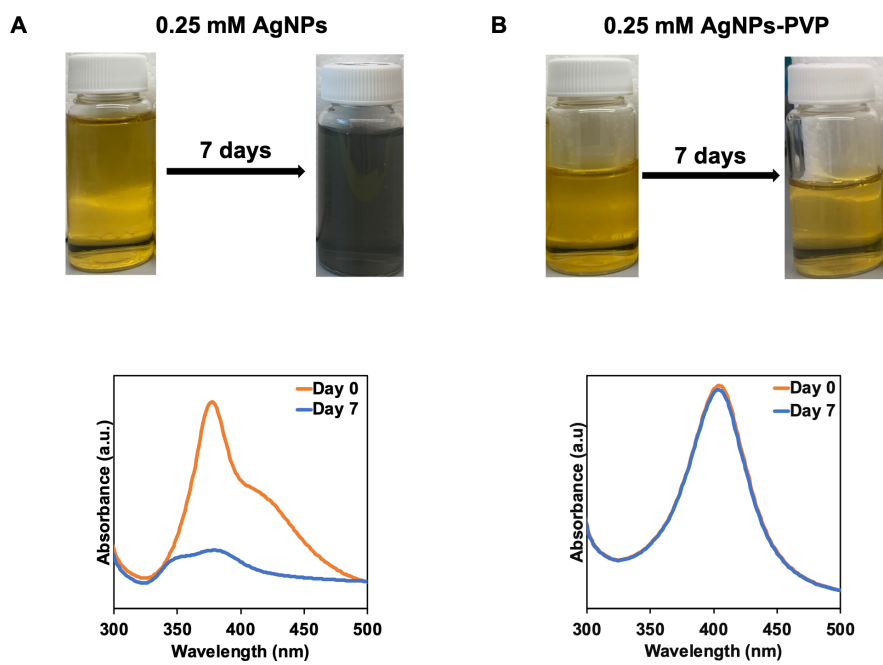
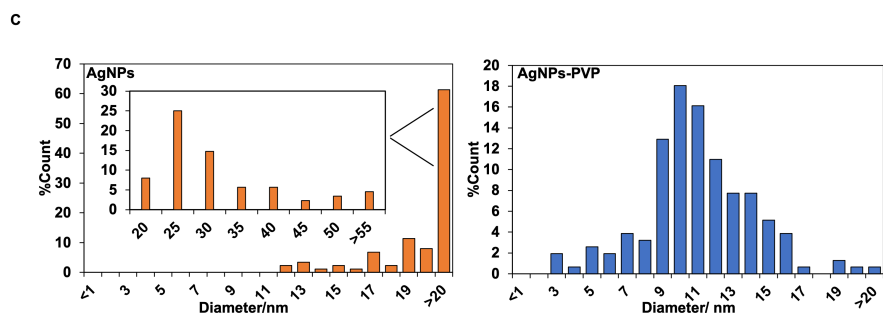
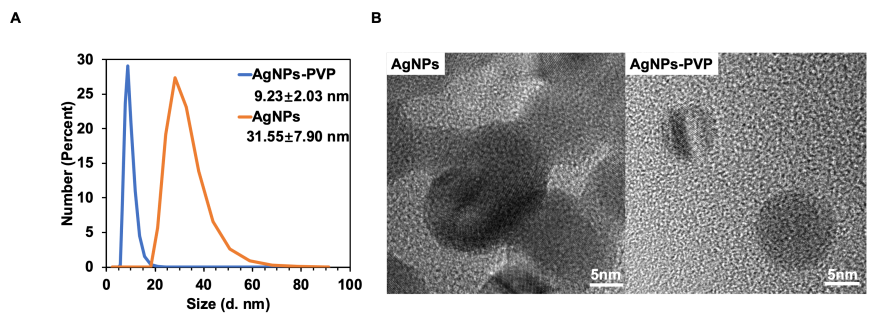
14. Rai MK, Deshmukh SD, Ingle AP, Gade AK. Silver nanoparticles: The powerful nanoweapon against multidrug-resistant bacteria. *J Appl Microbiol* . 2012;112(5):841-852. doi:10.1111/j.1365-2672.2012.05253.x
15. Kim JS, Kuk E, Yu KN, et al. Antimicrobial effects of silver nanoparticles. *Nanomedicine Nanotechnology, Biol Med* . 2007;3(1):95-101. doi:10.1016/j.nano.2006.12.001
16. Qing Y, Cheng L, Li R, et al. Potential antibacterial mechanism of silver nanoparticles and the optimization of orthopedic implants by advanced modification technologies. *Int J Nanomedicine* . 2018;13:3311-3327. doi:10.2147/IJN.S165125
17. Murray RGE, Steed P, Elson HE. the Location of the Mucopeptide in Sections. *Can J Microbiol* . 1965;11(December 1963):547-560.
18. Lancee B. The Negative Side Effects of Vocational Education. *Am Behav Sci* . 2016;60(5-6):659-679. doi:10.1177/0002764216632835
19. Budama L, Çakir BA, Topel Ö, Hoda N. A new strategy for producing antibacterial textile surfaces using silver nanoparticles. *Chem Eng J* . 2013;228:489-495. doi:10.1016/j.cej.2013.05.018
20. Shockman GD, Barrett JF. Structure, function, and assembly of cell walls of gram-positive bacteria. *Annu Rev Microbiol* . 1983;37:501-527. doi:10.1146/annurev.mi.37.100183.002441
21. Gupta P, Bajpai M, Bajpai SK. Textile technology: Investigation of antibacterial properties of silver nanoparticle-loaded poly (acrylamide-co-itaconic acid)-grafted cotton fabric. *J Cotton Sci* . 2008;12(3):280-286.
22. Manke A, Wang L, Rojanasakul Y. Mechanisms of nanoparticle-induced oxidative stress and toxicity. *Biomed Res Int* . 2013;2013. doi:10.1155/2013/942916
23. Roy A, Bulut O, Some S, Mandal AK, Yilmaz MD. Green synthesis of silver nanoparticles: Biomolecule-nanoparticle organizations targeting antimicrobial activity. *RSC Adv* . 2019;9(5):2673-2702. doi:10.1039/c8ra08982e
24. Hamida RS, Ali MA, Goda DA, Khalil MI, Al-Zaban MI. Novel Biogenic Silver Nanoparticle-Induced Reactive Oxygen Species Inhibit the Biofilm Formation and Virulence Activities of Methicillin-Resistant Staphylococcus aureus (MRSA) Strain. *Front Bioeng Biotechnol* . 2020;8(May):1-14. doi:10.3389/fbioe.2020.00433
25. Samuel MS, Jose S, Selvarajan E, Mathimani T, Pugazhendhi A. Biosynthesized silver nanoparticles using *Bacillus amyloliquefaciens*; Application for cytotoxicity effect on A549 cell line and photocatalytic degradation of p-nitrophenol. *J Photochem Photobiol B Biol* . 2020;202(August 2019):111642. doi:10.1016/j.jphotobiol.2019.111642
26. Tian J, Wong KKY, Ho CM, et al. Topical delivery of silver nanoparticles promotes wound healing. *ChemMedChem* . 2007;2(1):129-136. doi:10.1002/cmdc.200600171
27. Santoro CM, Duchsherer NL, Grainger DW. Minimal in vitro antimicrobial efficacy and ocular cell toxicity from silver nanoparticles. *Nanobiotechnology* . 2007;3(2):55-65. doi:10.1007/s12030-008-9007-z
28. Totaro P, Rambaldini M. Efficacy of antimicrobial activity of slow release silver nanoparticles dressing in post-cardiac surgery mediastinitis. *Interact Cardiovasc Thorac Surg* . 2009;8(1):153-154. doi:10.1510/icvts.2008.188870
29. Austin LA, Kang B, Yen CW, El-Sayed MA. Plasmonic imaging of human oral cancer cell communities during programmed cell death by nuclear-targeting silver nanoparticles. *J Am Chem Soc* . 2011;133(44):17594-17597. doi:10.1021/ja207807t
30. He X, Peng C, Qiang S, et al. Less is more: Silver-AIE core@shell nanoparticles for multimodality cancer imaging and synergistic therapy. *Biomaterials* . 2020;238(February):119834. doi:10.1016/j.biomaterials.2020.119834

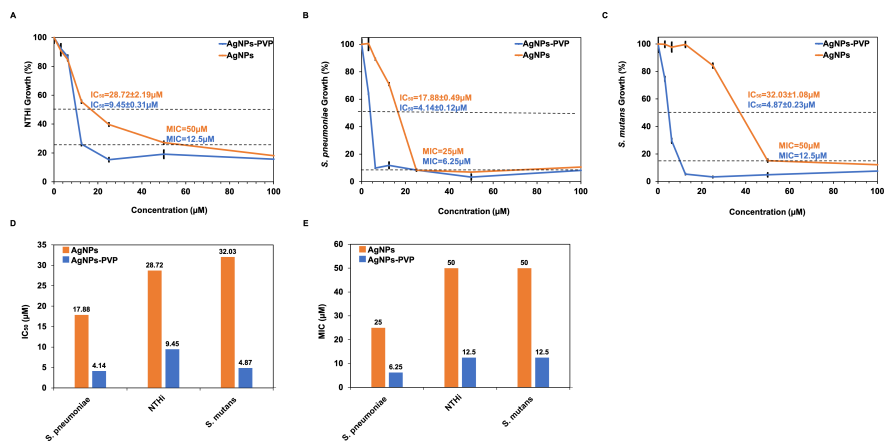
31. He D, Garg S, Waite TD. H₂O₂-mediated oxidation of zero-valent silver and resultant interactions among silver nanoparticles, silver ions, and reactive oxygen species. *Langmuir* . 2012;28(27):10266-10275. doi:10.1021/la300929g
32. Aabdallah M, Bayoumy A, Ibrahim A. Antimicrobial Activity and Synergistic Antimicrobial Potential of Silver Nanoparticles against microbial contaminants isolated from pharmaceutical production areas. *Res J Appl Biotechnol* . 2019;5(1):86-98. doi:10.21608/rjab.2019.76899
33. Alkawareek MY, Bahloul A, Abulatefeh SR, Alkilany AM. Synergistic antibacterial activity of silver nanoparticles and hydrogen peroxide. *PLoS One* . 2019;14(8):1-12. doi:10.1371/journal.pone.0220575
34. Hoare TR, Kohane DS. Hydrogels in drug delivery: Progress and challenges. *Polymer (Guildf)* . 2008;49(8):1993-2007. doi:10.1016/j.polymer.2008.01.027
35. Michida N, Hayashi M, Hori T. Comparison of event related potentials with and without hypnagogic imagery. *Psychiatry Clin Neurosci* . 1998;52(2):145-147. doi:10.1111/j.1440-1819.1998.tb00997.x
36. Moawad FA, Ali AA, Salem HF. Nanotransfersomes-loaded thermosensitive in situ gel as a rectal delivery system of tizanidine HCL: Preparation, in vitro and in vivo performance. *Drug Deliv* . 2017;24(1):252-260. doi:10.1080/10717544.2016.1245369
37. Liu Y, Wang X, Liu Y, Di X. Thermosensitive In Situ Gel Based on Solid Dispersion for Rectal Delivery of Ibuprofen. *AAPS PharmSciTech* . 2018;19(1):338-347. doi:10.1208/s12249-017-0839-5
38. Koffi AA, Agnely F, Ponchel G, Grossiord JL. Modulation of the rheological and mucoadhesive properties of thermosensitive poloxamer-based hydrogels intended for the rectal administration of quinine. *Eur J Pharm Sci* . 2006;27(4):328-335. doi:10.1016/j.ejps.2005.11.001
39. Sridhar V, Wairkar S, Gaud R, Bajaj A, Meshram P. Brain targeted delivery of mucoadhesive thermosensitive nasal gel of selegiline hydrochloride for treatment of Parkinson's disease. *J Drug Target* . 2018;26(2):150-161. doi:10.1080/1061186X.2017.1350858
40. Mura P, Mennini N, Nativi C, Richichi B. In situ mucoadhesive-thermosensitive liposomal gel as a novel vehicle for nasal extended delivery of opiorphin. *Eur J Pharm Biopharm* . 2018;122(October 2017):54-61. doi:10.1016/j.ejpb.2017.10.008
41. Mirza MA, Panda AK, Asif S, et al. A vaginal drug delivery model. *Drug Deliv* . 2016;23(8):3123-3134. doi:10.3109/10717544.2016.1153749
42. Rençber S, Karavana SY, Şenyiğit ZA, Eraç B, Limoncu MH, Baloğlu E. Mucoadhesive in situ gel formulation for vaginal delivery of clotrimazole: formulation, preparation, and in vitro/in vivo evaluation. *Pharm Dev Technol* . 2017;22(4):551-561. doi:10.3109/10837450.2016.1163385
43. Giuliano E, Paolino D, Fresta M, Cosco D. Mucosal applications of poloxamer 407-based hydrogels: An overview. *Pharmaceutics* . 2018;10(3):1-26. doi:10.3390/pharmaceutics10030159
44. Rana AK, Upadhyay D, Yadav A, Prasad S. Correlation of Tympanic Membrane Perforation with Hearing Loss and Its Parameters in Chronic Otitis Media: An Analytical Study. *Indian J Otolaryngol Head Neck Surg* . 2020;72(2):187-193. doi:10.1007/s12070-019-01740-9
45. Marchisio P, Esposito S, Baggi E, et al. Prospective evaluation of the aetiology of acute otitis media with spontaneous tympanic membrane perforation. *Clin Microbiol Infect* . 2017;23(7):486.e1-486.e6. doi:10.1016/j.cmi.2017.01.010
46. Mirzaei A, Janghorban K, Hashemi B, Bonyani M, Leonardi SG, Neri G. Characterization and optical studies of PVP-capped silver nanoparticles. *J Nanostructure Chem* . 2017;7(1):37-46. doi:10.1007/s40097-016-0212-3

47. Solomon SD, Bahadory M, Jeyarajasingam A V., Rutkowsky SA, Boritz C, Mulfinger L. Synthesis and study of silver nanoparticles. *J Chem Educ* . 2007;84(2):322-325. doi:10.1021/ed084p322
48. Starner TD, Zhang N, Kim GH, Apicella MA, McCray PB. Haemophilus influenzae forms biofilms on airway epithelia: Implications in cystic fibrosis. *Am J Respir Crit Care Med* . 2006;174(2):213-220. doi:10.1164/rccm.200509-1459OC
49. Barbosa JO, Rossoni RD, Vilela SFG, et al. Streptococcus mutans can modulate biofilm formation and attenuate the virulence of Candida Albicans. *PLoS One* . 2016;11(3):1-16. doi:10.1371/journal.pone.0150457
50. Quintero Moreno B, Araque M, Mendoza E. Evaluation of Two Supplemented Culture Media for Long-Term, Room-Temperature Preservation of Streptococcus pneumoniae Strains. *Biomed Res Int* . 2017;2017:1218798. doi:10.1155/2017/1218798
51. Yang R, Sabharwal V, Okonkwo OS, et al. Treatment of otitis media by transtympanic delivery of antibiotics. *Sci Transl Med* . 2016;8(356):1-11. doi:10.1126/scitranslmed.aaf4363
52. Manikam VR, Cheong KY, Razak KA. Chemical reduction methods for synthesizing Ag and Al nanoparticles and their respective nanoalloys. *Mater Sci Eng B Solid-State Mater Adv Technol* . 2011;176(3):187-203. doi:10.1016/j.mseb.2010.11.006
53. Sun Y, Liu Y, Guizhe Z, Zhang Q. Effects of hyperbranched poly(amido-amine)s structures on synthesis of Ag particles. *J Appl Polym Sci* . 2008;107(1):9-13. doi:10.1002/app.26132
54. Cloutier CR, Alfantazi A, Gyenge E. Physicochemical properties of alkaline aqueous sodium metaborate solutions. *J Fuel Cell Sci Technol* . 2007;4(1):88-98. doi:10.1115/1.2393310
55. Zhang Z, Zhao B, Hu L. PVP protective mechanism of ultrafine silver powder synthesized by chemical reduction processes. *J Solid State Chem* . 1996;121(1):105-110. doi:10.1006/jssc.1996.0015
56. Chou K Sen, Ren CY. Synthesis of nanosized silver particles by chemical reduction method. *Mater Chem Phys* . 2000;64(3):241-246. doi:10.1016/S0254-0584(00)00223-6
57. Sadeghi B, Pourahmad A. Effects of protective agents (PVA & PVP) on the formation of silver nanoparticles. *Int J Nanosci Nanotechnol* . 2008;4(1):3-12.
58. Magdassi S, Bassa A, Vinetsky Y, Kamyshny A. Silver nanoparticles as pigments for water-based ink-jet inks. *Chem Mater* . 2003;15(11):2208-2217. doi:10.1021/cm021804b
59. Xu Y, Li S, Yue X, Lu W. Nanosilver-cellulose antibacterials. *BioResources* . 2018;13(1):2150-2170.
60. Pabisch S, Feichtenschlager B, Kickelbick G, Peterlik H. Effect of interparticle interactions on size determination of zirconia and silica based systems - A comparison of SAXS, DLS, BET, XRD and TEM. *Chem Phys Lett* . 2012;521:91-97. doi:10.1016/j.cplett.2011.11.049
61. Fissan H, Ristig S, Kaminski H, Asbach C, Epple M. Comparison of different characterization methods for nanoparticle dispersions before and after aerosolization. *Anal Methods* . 2014;6(18):7324-7334. doi:10.1039/c4ay01203h
62. Reimche JL, Kirse DJ, Whigham AS, Swords WE. Resistance of non-typeable Haemophilus influenzae biofilms is independent of biofilm size. *Pathog Dis* . 2017;75(1):1-11. doi:10.1093/femspd/ftw112
63. Pericone CD, Overweg K, Hermans PWM, Weiser JN. Inhibitory and bactericidal effects of hydrogen peroxide production by Streptococcus pneumoniae on other inhabitants of the upper respiratory tract. *Infect Immun* . 2000;68(7):3990-3997. doi:10.1128/IAI.68.7.3990-3997.2000
64. Carlsson J, Iwami Y, Yamada T. Hydrogen peroxide excretion by oral streptococci and effect of lactoperoxidase-thiocyanate-hydrogen peroxide. *Infect Immun* . 1983;40(1):70-80. doi:10.1128/iai.40.1.70-80.1983

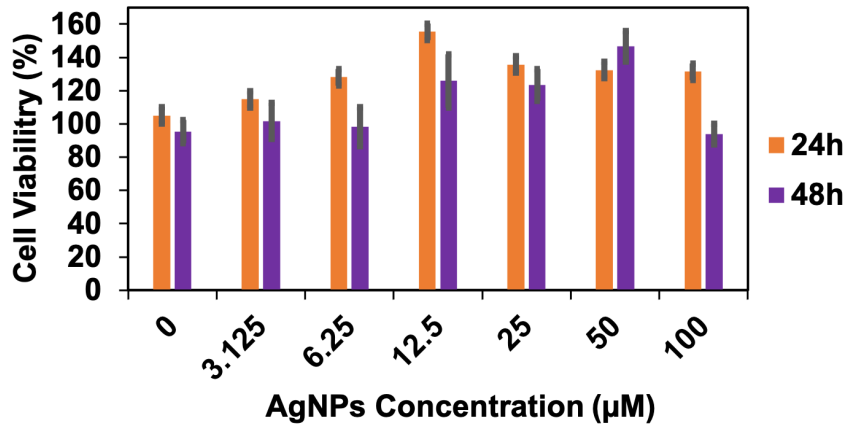
65. Thomas EL, Pera KA. Oxygen metabolism of *Streptococcus mutans*: Uptake of oxygen and release of superoxide and hydrogen peroxide. *J Bacteriol* . 1983;154(3):1236-1244. doi:10.1128/jb.154.3.1236-1244.1983
66. Banas JA. Virulence properties of *Streptococcus mutans*. *Front Biosci* . 2004;9(June):1267-1277. doi:10.2741/1305
67. Kashyap N, Katlam T, Avinash A, Kumar B, Kulshrestha R, Das P. Middle ear infection in children and its association with dental caries. *Med Pharm Reports* . 2019;92(3):271-276. doi:10.15386/cjmed-1043
68. Baldeck JD, Marquis RE. Targets for hydrogen-peroxide-induced damage to suspension and biofilm cells of *Streptococcus mutans*. *Can J Microbiol* . Published online 2008.
69. Li D, Nie W, Chen L, et al. Fabrication of curcumin-loaded mesoporous silica incorporated polyvinyl pyrrolidone nanofibers for rapid hemostasis and antibacterial treatment. *RSC Adv* . 2017;7(13):7973-7982. doi:10.1039/c6ra27319j
70. Setiyorini Y, Lou X, Pintowantoro S. The Influence of Temperature and Drug Concentrations Prednisolone in NIPAAm Copolymer. *Procedia Chem* . 2012;4:336-342. doi:10.1016/j.proche.2012.06.047
71. Dear SP, Saunders JC. Middle ear structure in the chinchilla: A quantitative study. *Am J Otolaryngol - Head Neck Med Surg* . 1988;9(2):58-67. doi:10.1016/S0196-0709(88)80009-7



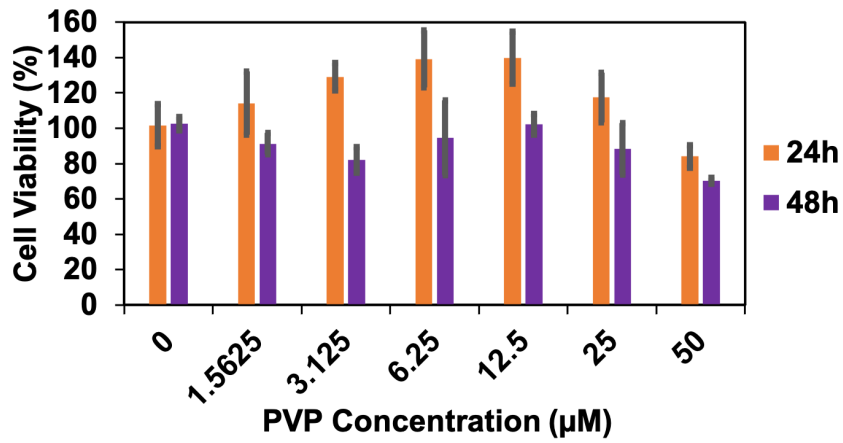




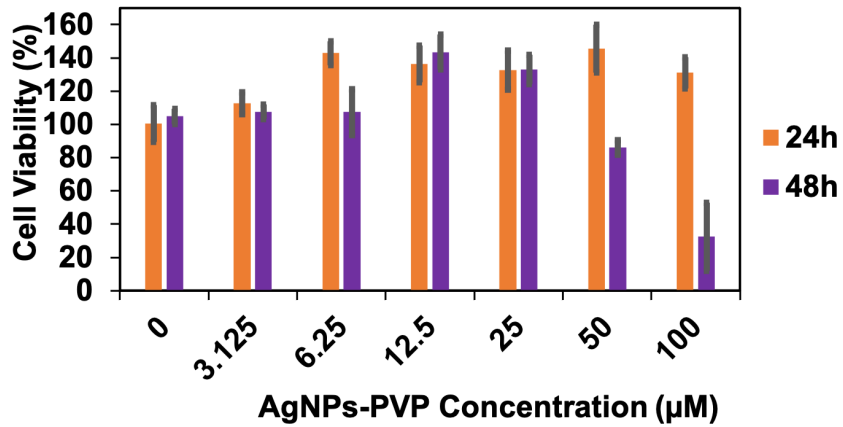
A

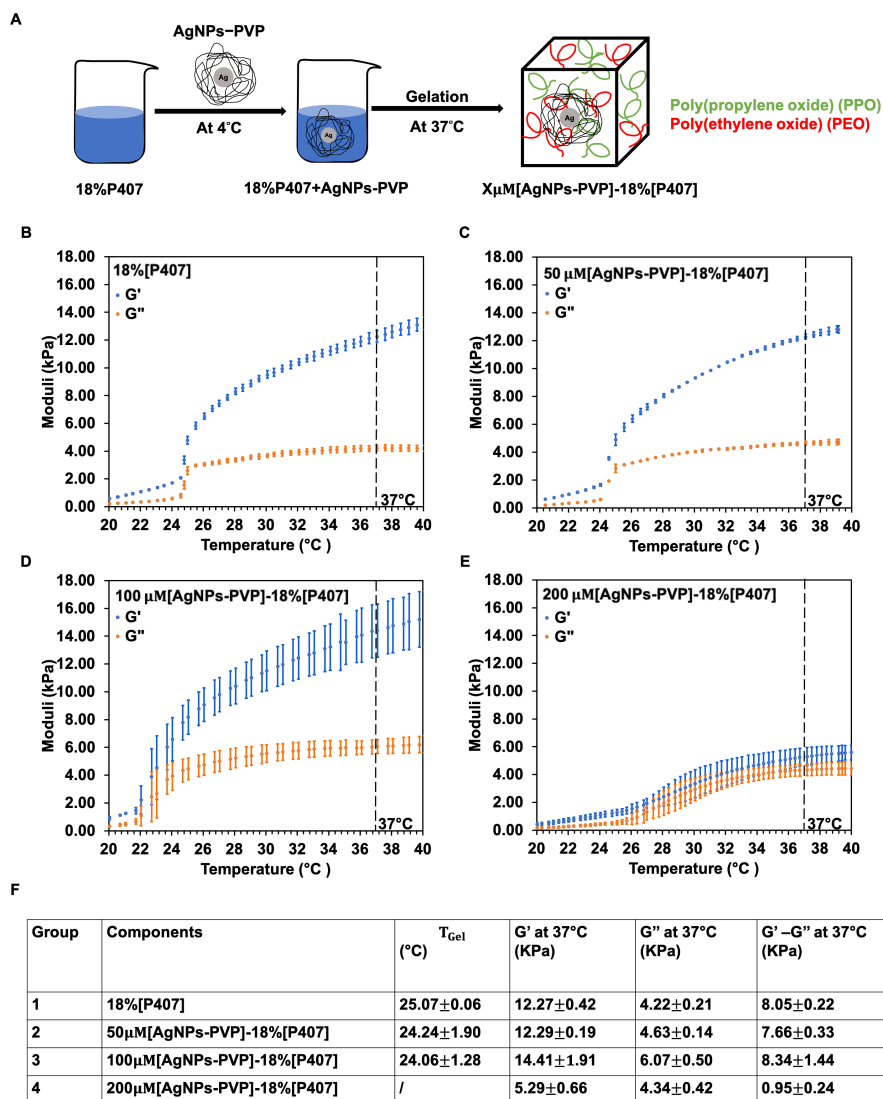


B

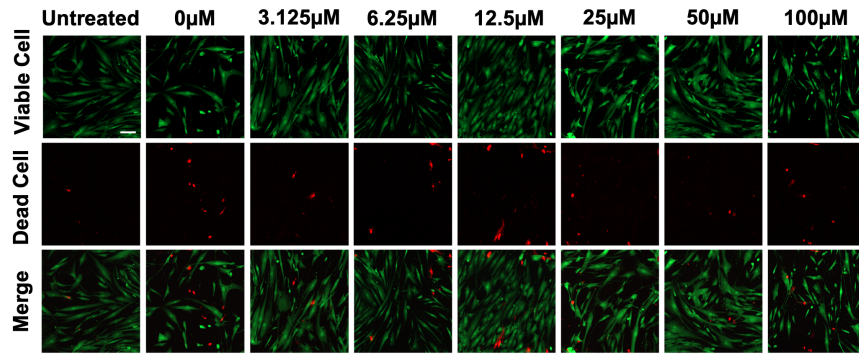


C





A



B

